

Real-Time Image Segmentation via Hybrid Convolutional-Transformer Architecture Search

Hongyuan Yu¹, Cheng Wan², Xiyang Dai^{5*}, Mengchen Liu⁵, Dongdong Chen⁵, Bin Xiao⁵, Yan Huang^{3,4}, Yuan Lu⁵, Liang Wang^{3,4}

¹*The Multimedia Department, Xiaomi Inc. (XIAOMI)*

²*Georgia Institute of Technology (GATECH)*

³*Center for Research on Intelligent Perception and Computing (CRIPAC),*

National Laboratory of Pattern Recognition (NLPR)

⁴*University of Chinese Academy of Sciences (UCAS)*

⁵*Microsoft Inc.*

yuhuayan1995@gmail.com

cwan38@gatech.edu

cddlyf@gmail.com

{yhuang, wangliang}@nlpr.ia.ac.cn

{mengcliu, docheng, bin.xiao, luyuan, xiyang.dai}@microsoft.com

Abstract

Image segmentation is one of the most fundamental problems in computer vision and has drawn a lot of attention due to its vast applications in image understanding and autonomous driving. However, designing effective and efficient segmentation neural architectures is a labor-intensive process that may require numerous trials by human experts. In this paper, we address the challenge of integrating multi-head self-attention into high-resolution representation CNNs efficiently by leveraging architecture search. Manually replacing convolution layers with multi-head self-attention is non-trivial due to the costly overhead in memory to maintain high resolution. By contrast, we develop a multi-target multi-branch supernet method, which not only fully utilizes the advantages of high-resolution features but also finds the proper location for placing the multi-head self-attention module. Our search algorithm is optimized towards multiple objectives (e.g., latency and mIoU) and is capable of finding architectures on the Pareto frontier with an arbitrary number of branches in a single

*Corresponding author

search. We further present a series of models via the Hybrid Convolutional-Transformer Architecture Search (HyCTAS) method that searches for the best hybrid combination of light-weight convolution layers and memory-efficient self-attention layers between branches from different resolutions and fuses them to high resolution for both efficiency and effectiveness. Extensive experiments demonstrate that HyCTAS outperforms previous methods in both semantic segmentation and panoptic segmentation tasks. Code and models are available at <https://github.com/MarvinYu1995/HyCTAS>.

Keywords: segmentation, high-resolution, neural architecture search, attention

1. Introduction

Image segmentation predicts pixel-level annotations of different semantic categories for an image. Unlike image classification, which assigns a single label for an entire image, image segmentation requires a per-pixel label, making it a core challenge in tasks such as autonomous driving, medical image analysis, and general scene understanding. Specifically, semantic segmentation assigns each pixel to one of several predefined categories (e.g., sky, tree, human, car), instance segmentation differentiates individual object instances of the same category, and panoptic segmentation [1] unifies these two perspectives by assigning each pixel a class label and an instance identity.

Over the past decade, deep neural networks have revolutionized segmentation performance [2, 3]. In particular, high-resolution representation architectures (e.g., HRNet [4, 5]) have significantly boosted accuracy by preserving spatial details throughout the network. However, these improvements often come at the cost of high computational overhead. Manually designing a segmentation framework that retains fine spatial features, incorporates global context (e.g., via attention mechanisms), and still runs in real time is notoriously difficult.

Recently, transformer-based models [11, 12] have shown promise in vision tasks by modeling long-range dependencies. Yet, straightforwardly replacing convolutional layers with self-attention can be impractical for high-resolution

Table 1: **Comparisons with state-of-the-art search methods** [6, 7, 8, 9, 10]. In these comparisons, ρ and τ represent the Pearson Correlation Coefficient and the Kendall Rank Correlation Coefficient of the true accuracy (by training each of them from scratch) and estimated accuracy (predicted by the super-network). **Memory Cost** reports the GPU memory consumption during the search process, **GPU Days** presents the searching cost, and **Nums** reports the number of the discovered architectures.

Method	GPU Days	Memory Cost	Nums	$\rho \uparrow$	$\tau \uparrow$
Auto-DeepLab [6]	3	Total supernet	1	0.31	0.21
FasterSeg [7]	2	Total supernet	1	0.35	0.25
SparseMask [8]	4.2	Total supernet	1	0.49	0.38
DPC [9]	2600	One subnet	1	0.46	0.37
Fast-NAS [10]	8	One subnet	1	0.42	0.33
HyCTAS(Ours)	5	One subnet	multiple	0.79	0.58

segmentation due to quadratic complexity in both computation and memory. To achieve truly efficient, real-time segmentation, we believe it is crucial to combine:

- *Lightweight convolutions*, which preserve spatial detail while limiting computational load.
- *Memory-efficient self-attention*, which expands the receptive field and captures global dependencies without exploding memory usage.

In this paper, we propose a **Hybrid Convolutional-Transformer Architecture Search (HyCTAS)** framework to *automatically* discover powerful yet efficient segmentation networks. Rather than performing a manual, trial-and-error insertion of self-attention layers into a high-resolution CNN, HyCTAS leverages a multi-branch supernet search space and a genetic-based multi-objective optimization strategy. By jointly optimizing for latency and accuracy (mIoU), HyCTAS identifies an optimal “mix” of convolution and attention at multiple scales and resolutions. As a result, we obtain a family of architectures that lie on the Pareto frontier of speed and performance.

Our key contributions can be summarized as:

- **Novel multi-branch search framework:** We encode parallel CNN branches at multiple resolutions, each of which may contain either lightweight convolution or memory-efficient attention. This unified supernet preserves high-resolution feature streams while optimizing for real-time inference.
- **Flexible multi-objective optimization:** We employ a genetic-based algorithm to search for efficient architectures that yield a range of trade-offs between speed (latency) and segmentation accuracy (mIoU). Importantly, we can discover multiple Pareto-optimal architectures *in a single search*.
- **Strong performance on multiple tasks:** Extensive experiments on benchmarks such as Cityscapes, ADE20K, and COCO demonstrate that our searched models consistently outperform prior works in semantic and panoptic segmentation—while significantly reducing computational cost and increasing inference speed.

2. Related Work

2.1. Efficient Networks for Image Segmentation

Semantic segmentation has long benefited from fully convolutional networks [13], which effectively adapt classification backbones to dense prediction tasks. Subsequent refinements, such as atrous/dilated convolutions in DeepLab [14] and multi-branch high-resolution designs in HRNet [4, 5], steadily pushed performance. Meanwhile, real-time or low-complexity methods such as ICNet [15], BiSeNet [16], and Fast-SCNN [17] introduced architectural optimizations (e.g., factorized convolutions, multi-resolution branches) to reduce latency. In more recent works, lightweight backbone designs [18, 19] target embedded devices and further illustrate the trade-off between efficiency and accuracy.

Unlike most prior approaches that *manually* reduce resolution or remove branches to save compute, our HyCTAS approach *searches* across multi-resolution sub-networks, identifying the best structure automatically. This not only exploits the advantages of high-resolution representations but also finds the optimal placement of memory-efficient self-attention modules.

Table 2: The difference between a typical operation and the proposed efficient operation. FLOPs are measured using an input of size $1 \times 256 \times 32 \times 64$. The receptive field (RF) is relatively compared with the standard convolution.

Operation Type	FLOPs (G)	Params (M)	RF	Scale-to-Input
Convolution	1.2	0.59	1	Linear
Light-weight Convolution	0.4	0.66	2	Linear
Transformer	4.3	12.62	<i>Max</i>	Quadratic
Memory-efficient Self-attention	0.6	0.81	<i>Max</i>	Quadratic

2.2. Neural Architecture Search

Neural Architecture Search (NAS) has emerged to automate network design [20, 21]. Early NAS solutions often employed reinforcement learning or evolutionary algorithms to explore cell-based search spaces [22]. Although these methods can discover effective designs, their applicability to large-scale semantic segmentation has been limited by high computational overhead.

Recent works have extended NAS to semantic segmentation [23, 6, 7, 24], but many still rely on a single-path or single-resolution paradigm. Our HyCTAS goes further by accommodating *multiple branches* (with varying spatial resolutions) within one unified supernet. Moreover, our multi-objective search can discover a *set* of Pareto-optimal architectures—each balancing accuracy and speed differently—in a single pass.

2.3. Transformer in Vision Tasks

Transformers [25] originally showed remarkable success in NLP, and have recently gained popularity in vision tasks. Fully attentional backbones like Vision Transformer [11] and SETR [12] capture global context effectively but incur high memory costs, especially for large input resolutions. Hybrid strategies like DETR [26] combine CNNs with transformers for detection and segmentation.

We follow the hybrid philosophy, blending lightweight convolutions with a *memory-efficient self-attention* module. Crucially, we do not merely handcraft these combinations; our search algorithm determines the *where* and *when* to use

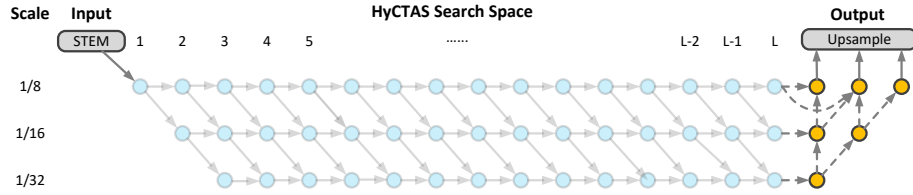


Figure 1: An illustration of our HyCTAS search space. It preserves the multi-resolution and multi-branch properties of HRNet by introducing two types of searchable components: cells and nodes, which extend HRNet with multi-module fusion ability.

attention across multiple scales, striking a better balance between accuracy and runtime efficiency.

3. Proposed Approach

3.1. Overall Workflow

Our HyCTAS framework can be summarized in four main steps:

1. **Supernet Construction:** We construct a multi-branch supernet inspired by HRNet, preserving parallel streams at various resolutions (e.g., 1/8, 1/16, 1/32). In each layer, we introduce *searchable cells* (for choosing lightweight convolution or memory-efficient self-attention) and *searchable nodes* (for fusion and skip connections).
2. **Supernet Training:** We randomly sample sub-networks from the supernet during training. To ensure coverage of multi-resolution paths, we bias the sampling probabilities so that deeper or wider sub-networks still appear sufficiently often.
3. **Multi-Objective Search:** Once the supernet weights are trained, we evaluate candidate sub-networks by measuring both segmentation accuracy (mIoU) and latency. We formulate a multi-objective problem and adopt an evolutionary algorithm (NSGA-II) to efficiently traverse the architecture space.

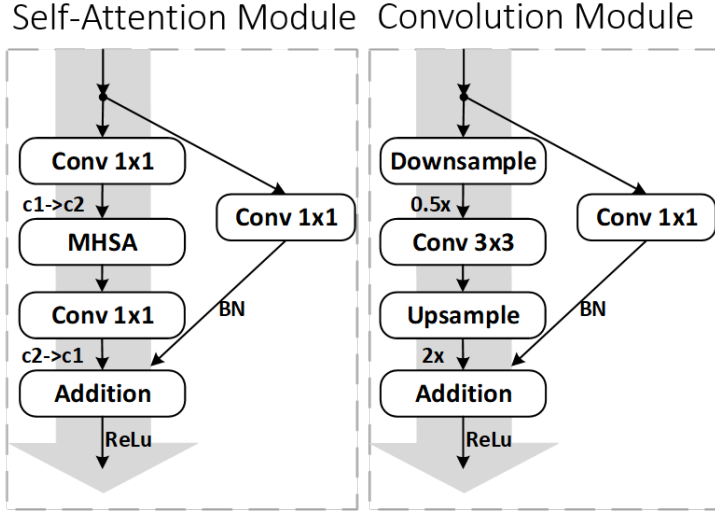


Figure 2: An illustration of our searchable modules. We design a memory-efficient self-attention module and a lightweight convolution module and search for the best combination.

4. **Architecture Selection:** The search yields a set of Pareto-optimal architectures, each offering a distinct trade-off (e.g., ultra-fast inference vs. higher accuracy). We finally retrain the chosen models from scratch to confirm their performance.

3.2. Revisiting HRNet Architecture

Learning high-resolution representations is crucial for good performance in image segmentation. HRNet achieves this by maintaining **multi-branch** convolution streams in parallel to preserve high-resolution representations throughout the whole network and generates reliable high-resolution representations with strong position sensitivity through repeatedly fusing the representations from **multi-resolution** streams.

In order to preserve these two key properties, we design our HyCTAS supernet to enable searching for variant branch numbers, depths, widths, and spatial resolutions all in one. As shown in Figure 1, our supernet contains two types of searchable components: Cells and Nodes.

Given a supernet with L layers, after an input image goes through the initial stem layers, the feature resolutions are downsampled to strides $S = \{1/8, 1/16, 1/32\}$ and fed into multiple searchable cells $C = \{C_s^1, C_s^2, \dots, C_s^L\}$. Then the features are fused into searchable nodes $N = \{N_s^1, N_s^2, \dots, N_s^{L-1}\}$ consecutively, where the cells and nodes are alternately stacked. The searching domain is different for cells and nodes. A cell could contain multiple modules such as convolution, transformer, and so on, which extends the network to be capable of combining **multi-module** into a sub-network. Meanwhile, a node is dedicated to fusing multiple branches from different resolutions together and behaves as a binary gate.

Since our architecture needs to support arbitrary branch fusion, the outputs of each architecture are not fixed, *i.e.*, the number of the last feature map channels and the branch position of the final outputs are not fixed. To solve these problems, we propose a feature aggregation head module that can adapt to arbitrary outputs of different architectures. The feature map of shape $(C_* \times H \times W)$ is first adjusted in channels by a 1×1 Slimmable Convolution layer [27] to the shape of $(C_s \times H \times W)$. If the feature map size is not the max resolution in the search space, it will be bilinearly upsampled to match the shape of the other feature map $(C_s \times 2H \times 2W)$. Then, the two feature maps are concatenated and fused together with a 3×3 convolution layer. We enumerate all the output combinations and set a head for each type of output F_θ , so there are a total of six different heads in our search space, *i.e.*, $\theta \in \{(8), (16), (32), (8, 16), (8, 32), (8, 16, 32)\}$.

Unlike previous works [6, 7] that limit the network search to one path, our HyCTAS supernet is capable of modeling sub-networks with arbitrary numbers of branches from different resolutions, which better captures the spirit of HRNet.

3.3. Combining Multiple Modules

Convolution facilitates the learning of visual features. With the weight-sharing mechanism, the features extracted from a convolutional layer are translation invariant. At the same time, the features are also locality-sensitive, where

every operation only takes into account a local region of the image. Thus, convolutional operations fail to encode relative spatial information and result in a limited receptive field.

However, large receptive fields are often required to track long-range dependencies within an image, which in practice involves using large kernels or long sequences of convolutional layers at the cost of losing efficiency. Recent works have presented the techniques of Transformers [25] to overcome the limitations presented by convolutional operations in an efficient way.

Transformers use the concept of multi-head self-attention. Such an attention mechanism models the importance between each pixel within the whole input, which results in a maximized receptive field. Compared with convolutional operations, transformers also have the problem of large computational overhead, especially when the feature map size is very large, as its computation and memory usage are quadratic to the input size.

Therefore, both operations do not meet our goal of pursuing efficiency if naively incorporated in our multi-resolution multi-branch framework for high-resolution image segmentation learning. Hence, we propose to use a memory-efficient self-attention module and a lightweight convolution module.

Memory-efficient Self-attention Module: Instead of directly borrowing typical transformer operations like previous works [12, 28], we only employ the self-attention layer [25] without the FFN to capture the global context while maximizing efficiency. We then use 1×1 convolutions for reducing and then increasing dimensions, leaving the self-attention module as a bottleneck with smaller than input/output channels. This largely reduces the memory usage required in the self-attention layer. Meanwhile, we add an extra bypassed 1×1 convolution module for preserving uncompressed residue. Our memory-efficient self-attention module operation can utilize the largest receptive field while keeping relatively small FLOPs and memory footprint.

Lightweight Convolution Module: To maintain a large receptive field while minimizing computational costs, methods like Zoomed Convolution [7] and Dilated Convolution [14] employ bilinear sampling for input feature map

resizing, inevitably leading to information loss. Addressing this, we introduce a novel, efficient convolution that incorporates a parallel 1×1 convolution to preserve high-resolution details, as shown in Figure 2. This approach connects the input feature map directly to the zoomed convolution’s output, effectively maintaining input resolution. Our lightweight convolution module significantly reduces information loss with minimal parameter increase, ensuring both speed and accuracy.

The detailed measurements of our memory-efficient self-attention module and lightweight convolution module are shown in Table 2. Properly combining the convolutional module and the self-attention module plays a significant role in improving model performance and efficiency. Hence, we further deploy a search algorithm to solve this problem.

3.4. Searching with Multi-objective

Inspired by [29], we formulate the search for the optimal architecture α^* as a two-stage optimization problem. The architecture search space \mathcal{A} is encoded in the supernet, denoted as $\mathcal{N}(\mathcal{A}, \mathcal{W})$. Each candidate architecture $\alpha \in \mathcal{A}$ shares its weights across \mathcal{W} . In the first stage, we optimize the supernet weights \mathcal{W} by:

$$\mathcal{W} = \arg \min_{\mathcal{W}} \mathcal{L}_{train}(\mathcal{N}(\mathcal{A}, \mathcal{W})) \quad (1)$$

where \mathcal{L}_{train} denotes the training loss.

The prior distribution of $\Gamma(\mathcal{A})$ is important. In order to meet our goal of searching for architectures with arbitrary branches from different resolutions, we pre-define this prior in the training process of the supernet. Since the sub-network with more branches contains the sub-network with fewer branches, we empirically set the sub-network with more branches to have a higher sampling probability.

$$\rho_i < \rho_{i+1}, \quad i \in \{1, 2, 3\} \quad (2)$$

where ρ_i means the sampling probability of architectures containing i branches. Other components in the sub-network α are sampled from a uniform distribution.

Once the supernet training is finished, the second stage is to search for architectures by ranking the accuracy and latency of each sub-network $\alpha \in \mathcal{A}$. We convert the architecture searching problem to a standard multi-objective optimization (MOP) problem.

The formulation consists of decision variables, objective functions, and constraints. The optimization objectives are as follows:

$$\begin{aligned}
 & \text{Maximize} \quad y = f(\alpha) = (f_1(\alpha), f_2(\alpha), \dots, f_k(\alpha)) \\
 & \text{S.t.} \quad e(x) = (e_1(\alpha), e_2(\alpha), \dots, e_m(\alpha)) \leq 0 \\
 & \text{among} \quad x = (\alpha_1, \alpha_2, \dots, \alpha_n) \in \mathcal{A} \\
 & \quad y = (y_1, y_2, \dots, y_k) \in Y
 \end{aligned} \tag{3}$$

Where α represents the decision vector, *i.e.*, the searched network architecture, y represents the target vector, *i.e.*, the mIoU and latency. \mathcal{A} represents the search space formed by the decision vector α , and Y represents the target space formed by the target vector y . The constraint $e(x) \leq 0$ determines the feasible value range of the decision vector. In order to ensure that the searched architectures are effective, we set the following four constraints: 1) The number of paths in each sub-network needs to be greater than 0; 2) For a sub-network that contains multiple paths, the locations of down-sampling should be different; 3) In the down-sampling position, skip connections cannot be selected; 4) The memory usage of a sub-network during training cannot exceed the hardware limit.

Different from the single-objective optimization problem, there is usually no unique optimal solution in an MOP problem, but a Pareto optimal solution set. Hence, we adapt the popular evolutionary algorithm NSGA-II [30] to solve the optimization problem. The details of our search algorithm can be found in the supplemental material.

The detailed search algorithm is presented in Algorithm 1. One-hot encoding

is employed to encode the sub-network α . When the sampling is over, we will decode the sub-network to evaluate its corresponding mIoU and latency. We solve this multi-objective optimization (MOP) problem under the NSGA-II [30] framework.

Algorithm 1 Multi-objective Search.

Input: supernet \mathcal{N} with weights \mathcal{W} , the number of branches b , the number of generations N , population size n , validation dataset D_{val} , objective weights w .

Output: K individual architectures on the Pareto front.

Uniformly generate the populations P_0 and Q_0 until each has n individuals architectures.

for $i = 0$ **to** $N - 1$ **do**

$R_i = P_i \cup Q_i$

$F, S = \text{Non-Dominated-Sorting}(R_i)$

 Pick n individual architectures to form P_{i+1} by ranks and the crowding distance weighted by w .

$Q_{i+1} = \emptyset$

while $\text{size}(Q_{i+1}) < n$ **do**

$M = \text{Tournament-Selection}(P_{i+1})$

$q_{i+1} = \text{Crossover}(M)$

if $\text{Latency}(q_{i+1}) > \text{Latency}(S_{max})$ **then**

 continue

end if

 Evaluate model q_{i+1} with S on D_{val}

if $\text{mIoU}(q_{i+1}) > \text{mIoU}_{min}$ **then**

 Add q_{i+1} to Q_{i+1}

end if

end while

end for

Select the best performing architecture from Pareto-front from P_N on D_{val} .

4. Experiments

We evaluate our method in both semantic segmentation task and the panoptic segmentation tasks. Panoptic segmentation was introduced by [31] to combine semantic and instance segmentation, in which all object instances are uniquely segmented to make the task even more challenging.

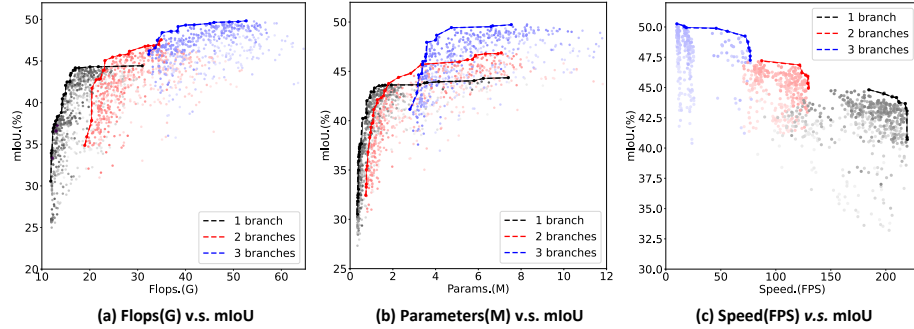


Figure 3: The searched architectures under different objectives on the Cityscapes validation set. Our proposed HyCTAS approach can search for multiple efficient architectures with arbitrary branches in a single run. The color from light to dark indicates that our search results are getting better and better as the search progresses. The solid line represents architectures on the Pareto frontier. Best viewed in color.

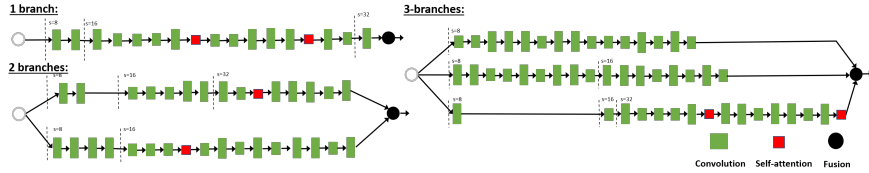


Figure 4: An illustration of our searched architectures with multiple branches.

4.1. Benchmark and Evaluation Metrics

Cityscapes [32] is a popular dataset that contains a diverse set of stereo video sequences recorded in street scenes from 50 different cities. It has 5,000 high-quality pixel-level annotations. There are 2,975 images for training, 500

images for validation, and 1,525 images without ground truth for testing to ensure a fair comparison. The dense annotation contains 19 classes for each pixel.

COCO [33] is a much larger and more challenging dataset for object detection and segmentation. There are a total of 133 classes, which include 80 'thing' and 53 'stuff' classes. We train our models on the train2017 set (118k images) and evaluate on the val2017 set (5k images).

ADE20K [34] has 20k images for training, 2k images for validation, and 3k images for testing. It is used in the ImageNet scene parsing challenge 2016 and has 150 classes and diverse scenes with 1,038 image-level annotations.

Evaluation Metrics. The mean intersection over union per class (mIoU), panoptic quality (PQ), and FPS (frames per second) are used as the metrics for semantic segmentation, panoptic segmentation, and speed, respectively.

4.2. Setup

Search. During training of the supernet, the sampling ratios for ρ_1 , ρ_2 , and ρ_3 are set to 0.2, 0.3, and 0.5, respectively. The initial channel count for the supernet is 64, and the mini-batch size is set to 16. The supernet is trained on the Cityscapes dataset with 256×512 images from the training set. We use the SGD optimizer with a momentum of 0.9 and a weight decay of 5×10^{-4} to optimize the supernet weights. The learning rate is set to 0.02 with an exponential learning rate decay of 0.992. The entire supernet optimization takes about 120 hours on a single V100 GPU.

In the search process, the initial population P_0 is set to 40 and generated by uniform random sampling. The probabilities of crossover and mutation operations are set at 0.9 and 0.02, respectively. Before the inference of a sub-network, the statistics of all Batch Normalization operations are recalculated on a random subset of training data (1000 images in Cityscapes). The number of generations is 20, and we search sub-networks with different branch numbers separately. Hence, a total of 2400 network sub-networks are searched.

Retrain. Similar to [6], we also use the filter multiplier to control the model

capacity, and the default values for HyCTAS-S and HyCTAS-L are set to 12 and 16, respectively. The final output stride of HyCTAS-S is 8, and the other big models’ final output strides are set to 4 by merging the low-level features in the stem. We use the SGD optimizer with a momentum of 0.9 and a weight decay of 5×10^{-4} to optimize the searched networks. The ‘poly’ learning rate policy is employed with an initial learning rate of 0.005. Data augmentations on all datasets, *i.e.*, random crop, flipping, etc., are consistent with [35]. On the Cityscapes dataset, the training images are cropped to 512×1024 and the mini-batch size is set to 32. It is worth noting that all our results are trained from scratch without ImageNet pretraining, and we only use the training set without any extra data.

Evaluation. We use an Nvidia GeForce RTX 3090 and an Intel Xeon E5-2680-v4 CPU (2.40GHz) for benchmarking the computation cost. When testing the inference speed, an image with a batch size of 1 is first loaded into the GPU memory and the model is warmed up to reach a steady speed. After that, the inference time is measured by running the model for six seconds. All the reported results, unless specified, are evaluated without multi-scale inference and flipping. The mean intersection over union per class (mIoU), panoptic quality (PQ) are used as the evaluation metrics for semantic segmentation and panoptic segmentation, respectively.

4.3. Model Exploration

We begin our experiments with the exploration of our searched architectures. As mentioned in the previous section, our search framework is capable of optimizing towards multiple different objectives. To better understand the architecture distributions under different objectives, we conduct three different searches, which cover the objectives “FLOPs vs. mIoU,” “Parameters vs. mIoU,” and “Speed vs. mIoU,” respectively. As shown in Figure 3, we visualize the evolution processes for different objectives. As our method is capable of searching sub-networks with an arbitrary number of branches, we visualize the group of architectures with different numbers of branches in different colors.

Table 3: Comparison of semantic segmentation on the Cityscapes. \dagger : speed on NVIDIA Xavier, \ddagger : speed with TensorRT acceleration, $*$: trained from scratch.

Methods	Input Size	mIoU (%) \uparrow		FLOPs \downarrow (G)	Params \downarrow (M)	Speed \uparrow (FPS)
		val	test			
ICNet [15]	1024x2048	67.7	69.5	-	-	37.7
BiSeNet [16]	768x1536	69.0	68.4	-	-	105.8
Fast-SCNN [17]	1024x2048	68.6	68.0	-	11.1	123.5
DF1-Seg-d8 [36]	1024x2048	72.4	71.4	-	-	136.9
HRNetV2 _{W18S} [5]	1024x2048	70.3	-	31.1	1.5	-
HRNetV2 _{W40} [5]	1024x2048	80.2	80.5	493.2	45.2	-
HyCTAS-S* (Ours)	1024x2048	72.3	73.0	13.0	1.5	159.2
CAS [23]	768x1536	71.6	70.5	-	-	108.0
MobileNetV3 [18]	-	72.4	72.6	9.7	1.5	10.8 \dagger
SqueezeNAS [37]	-	73.6	72.5	19.6	1.9	10.2 \dagger
FasterSeg [7]	1024x2048	73.1	71.5	28.2	4.4	149 \ddagger
SeaFormer-S [19]	1024x2048	70.7	71.0	2.0	-	7.7
SeaFormer-B [19]	1024x2048	72.2	72.5	3.4	-	4.8
HyCTAS-M* (Ours)	1024x2048	77.1	75.7	29.4	2.4	87.8
Dynamic _{L32} [24]	1024x2048	79.2	80.0	242.3	-	-
SETR _{PUP} [12]	768x768	79.3	-	318.3	-	-
Auto-DeepLab _L [*] [6]	1025x2049	80.3	80.4	695.0	44.4	0.5
OCR _{HRNetV2-W48} [28]	1024x2048	80.6	-	617.2	63.8	4.6
HyCTAS-L* (Ours)	1024x2048	80.9	79.4	527.0	43.2	12.4

We also plot the Pareto boundary at the end of the search. It is interesting to find out that searching for different objectives largely affects the architecture distributions. For the following experiments, we choose architectures on the Pareto boundary from searching under "Speed vs. mIoU" because of better model separation and closer alignment to real-world requirements.

We also visualize the searched architectures with multiple branches in Figure 4. It is interesting to observe how the self-attention module is placed under a different number of branches. When the number of branches is 1, the self-attention modules can be placed in higher resolution to increase the network's performance; when the number of branches is 3, the self-attention modules would be placed at a deeper stage to better fuse the features from multiple

Table 4: Comparisons of panoptic segmentation on Cityscapes validation set. \dagger : speed on Tesla V100-SXM2 GPU, \ddagger : test with multi-scale and flipping augmentation, $*$: trained from scratch.

Methods	Input Size	PQ (%)	AP (%)	mIoU (%)
TASCNet \dagger [38]	-	60.4	39.1	78.7
Panoptic FPN [31]	-	58.1	33.0	75.7
AUNet [39]	-	59.0	34.4	75.6
UPSNet [40]	1024x2048	59.3	33.3	75.2
UPSNet \dagger [40]	-	60.1	33.3	76.8
Seamless [41]	1025x2049	60.3	33.6	77.5
AdaptIS [42]	1024x2048	62.0	36.3	79.2
DeeperLab [43]	1025x2049	56.5	-	-
SSAP \ddagger [44]	-	61.1	37.3	-
<hr/>				
Panoptic-DeepLab _{<i>HRNet-W48</i>}	1025x2049	63.3	35.9	80.3
Panoptic-DeepLab _{<i>Xception-71</i>}	1025x2049	63.0	35.3	80.5
HyCTAS-L*	1024x2048	63.3	34.0	81.3
<hr/>				
Panoptic-DeepLab _{<i>Xception-71</i>} \dagger	-	64.1	38.5	81.5
HyCTAS-L‡*	-	64.8	36.8	81.8

branches. This phenomenon well aligns with self-attention’s advantages and limitations.

4.4. Comparison to SOTA Models

We compare our method with state-of-the-art methods on two popular benchmarks.

Cityscapes. As shown in Table 3, we can see that when the speed is more than 100 FPS, our model establishes new state-of-the-arts. HyCTAS-M consistently outperforms recent BiSeNet [16], Fast-SCNN [17], and DF1-Segd8 [36]. In particular, our HyCTAS-M achieves 77.1% mIoU on the Cityscapes validation set with 29.4G FLOPs and 2.4M parameters, surpassing HRNetV2-W18-Small-v1 by 6.8% with a similar model size. On the Cityscapes test set, our HyCTAS-M surpasses FasterSeg [7] by 4.2%. Moreover, the speed of our model

reaches an astonishing 87.8 FPS without TensorRT acceleration. Meanwhile, our HyCTAS-S has the smallest FLOPs and parameters and achieves the fastest inference speed at 159.2 FPS. This proves that our models are very competitive when deployed on real hardware.

Without any pretraining or knowledge distillation, our big model HyCTAS-L achieves 80.9 mIoU on the Cityscapes validation set, which is 0.6% higher than Auto-DeepLab [6], while using fewer FLOPs. Compared to the expert-designed HRNetV2-W40 [5], HyCTAS-L is still 0.7% ahead on the validation set with nearly 100G fewer FLOPs. Notably, the HyCTAS-L can still run at 12.4 FPS. Since we target fast semantic segmentation, we did not use dilated separable convolution for fast inference speed. Besides, the mIoU is measured without any evaluation augmentation like flipping or multi-scale.

Compared with recent NAS-related models, our method also has obvious advantages in search time and GPU memory overhead: 1) Thanks to our multi-objective searching strategy, our HyCTAS only takes 5 GPU days to search a series of models which can satisfy different demands, *i.e.*, low latency model or high-performance model. By contrast, other NAS methods can only search for one model at a time, so their search overhead will increase linearly as the number of searched models increases. 2) Our model also achieves better performance than the baseline NAS methods. For example, HyCTAS-M is 3.8% superior to FasterSeg [7] on the Cityscapes validation set.

Compared with the latest development of Transformer-like models [12, 28], our HyCTAS-L model can afford inference using a much larger image and requires fewer FLOPs respectively. This demonstrates the overall advantages of our architectures, which can better combine convolution and self-attention to maximize efficiency.

We also evaluate HyCTAS-L on the Cityscapes validation set with the original image resolution of 1024×2048 . In Table 4, we see the superior PQ and speed of our HyCTAS-L. Without any inference tricks, our HyCTAS-L achieves 63.3% PQ and 81.3% mIoU, which is comparable to Panoptic-Deeplab with the HRNet-W48 [5] backbone. However, our HyCTAS-L runs twice as fast as

Table 5: Comparison of semantic segmentation on the ADE20K.

Methods	Encoder	FLOPs (G)	Params (M)	Speed (FPS)	mIoU (%)
FCN [13]	MobileNetV2	39.6	9.8	64.4	19.7
PSPNet [45]	MobileNetV2	52.9	13.7	57.7	29.6
DeepLabV3+ [46]	MobileNetV2	69.4	15.4	43.1	34.0
SegFormer [47]	MiT-B0	8.4	3.8	50.5	37.4
FCN [13]	ResNet-101	275.7	68.6	14.8	41.4
EncNet [48]	ResNet-101	218.8	55.1	14.9	44.7
PSPNet [45]	ResNet-101	256.4	68.1	15.3	44.4
DeepLabV3+ [46]	ResNet-101	255.1	62.7	14.1	44.1
Auto-DeepLab [6]	NAS-F48-ASPP	-	-	-	44.0
HyCTAS(Ours)	HyCTAS-L	72.7	43.2	71.8	44.9

Panoptic-Deeplab with the HRNet-W48 backbone. When we use inference data augmentation, our method achieved the best results. Specifically, our HyCTAS-L surpasses Panoptic-Deeplab [35] by 0.7% on PQ and 0.3% on mIoU. These results are achieved with only Cityscapes fine-annotated images, without using any extra data (coarse-annotated images, COCO, ImageNet, etc.).

ADE20K. We further evaluate our HyCTAS-L on the ADE20K validation set with the original image resolution of 640×640 . From Table 5, we can see that our model is much smaller and faster than others. Specifically, our HyCTAS-L achieves 44.9% mIoU with 71.8 FPS, which is 0.9% better than Auto-DeepLab [6]. Compared to those models with a ResNet-101 [49] encoder, we also achieve leading performance while using less than half the FLOPs. For example, the FLOPs of our HyCTAS-L is 72.7G, which is less than half of that of DeepLabV3+ [46]. For the MobileNetV2 [50] encoder, we have similar FLOPs, but our HyCTAS-L surpasses DeepLabV3+ [46], PSPNet [45], and FCN [13] by more than 10%. Furthermore, our HyCTAS-L surpasses the latest SegFormer [47] by 7.3% while also running around 40% faster.

COCO. We employ the recent bottom-up panoptic segmentation framework [35] as our baseline. To ensure fast running speed, we remove the heavy

Table 6: Comparison of panoptic segmentation on the COCO *val2017* set. \dagger denotes the speed on Tesla V100-SXM2 GPU, and \ddagger denotes test with multi-scale and flipping augmentation.

Methods	Input Size	Speed (FPS)	PQ (%)	PQ Th (%)	PQ St (%)
Deeperlab _{MNV2} [43]	641x641	17.2 \dagger	27.9	-	-
Deeperlab _{Xception-71} [43]	641x641	10.6 \dagger	33.8	-	-
Panoptic-DeepLab _{MNV3} [35]	641x641	13.5 \dagger	29.5	-	-
Panoptic-DeepLab _{ResNet-50}	641x641	6.0 \dagger	35.2	-	-
HyCTAS-L	640x640	63.9	35.4	36.8	33.1
HyCTAS-L\ddagger	-	-	36.8	38.5	34.5

context module and decoder module in Panoptic-Deeplab, which are built based on Atrous Spatial Pyramid Pooling (ASPP) [14]. We further transfer the discovered architecture, *i.e.*, HyCTAS-L, from Cityscapes to train on COCO. To ensure the inference speed, we set the test size to 640×640 . Table 6 reveals that without sacrificing much accuracy, our HyCTAS-L achieves an FPS of 63.9. This high speed is over 90% faster than the closest competitor in FPS [43]. Meanwhile, we surpass Deeperlab-MNV2 [43] by a large margin, *i.e.*, 7.5% PQ. Compared to Panoptic-Deeplab-MNV3 [35], our HyCTAS-L surpasses it on multiple performance points with 5.9% PQ. When using multi-scale and flipping, we achieve the best PQ at 640×640 resolution, which is 1.6% better than Panoptic-Deeplab-ResNet-50 and 3.0% better than Deeperlab-Xception-71 [43].

4.5. Ablation

Compared to Random Sampling. To verify the effectiveness of our searching strategy, we compared our discovered architectures with randomly sampled architectures on the Cityscapes validation set. We randomly sampled 5 architectures with 1-3 branches each from the search space. The results are presented in Table 7, in which each value is the average result of 5 random architectures. The discovered one-branch architecture, Searched-1, outperforms the random one-branch architecture by 4.3% with a smaller model size. The

discovered Searched-2 and Searched-3 both surpass random architectures by more than 3%.

Robustness of Searching. We further conducted an ablation study by intentionally changing components to verify the searching robustness of our HyCTAS-M model. As shown in Table 8, we distorted the searched architectures by replacing all self-attention with convolution, replacing all convolution with self-attention, shifting self-attention to another position, and shifting self-attention to another branch, i.e., moving it to a random position on the same stride. It can be seen that our searched models consistently perform better than these variants, proving their robustness.

In summary, the architecture searched by HyCTAS can find a great trade-off between performance, model size, and latency.

Table 7: Ablation study on the randomly sampled architectures on the Cityscapes validation set.

Architectures	FLOPs (G)	Params (M)	mIoU (%)
Random-1	14.6 ± 1.2	1.5 ± 0.2	68.0 ± 3.9
Searched-1	9.6	1.5	72.3
Random-2	31.6 ± 1.0	2.0 ± 0.7	73.6 ± 1.8
Searched-2	22.4	3.2	77.
Random-3	391.5 ± 11.4	32.0 ± 4.8	77.6 ± 0.9
Searched-3	335.1	43.2	80.9

Table 8: Ablation study on the searched architectures on the Cityscapes validation set.

Architectures	FLOPs (G)	Params (M)	mIoU (%)
Searched	29.4	2.4	77.1
+ SA - > Conv.	23.1	2.8	75.6
+ Conv. - > SA	20.5	2.5	74.3
+ Shift SA Position	23.1	2.8	75.2
+ Shift SA Branch	22.5	2.6	75.6

Table 9: Experiments with different settings on the Cityscapes validation set. ‘SDP’ denotes Scheduled Drop Path.

#	Iter-186k	Iter-372k	SDP-0.1	SDP-0.2	mIoU(%)
1	✓				71.5
2	✓		✓		73.0
3	✓			✓	73.3
4		✓		✓	73.5

Retrain Settings. From Table 9, we can see that adding the scheduled drop path [6] improves the mIoU by 1.5%. When the scheduled drop path probability is set to 0.2, the performance is improved by 0.3%. In #4, we also study the effects of larger training iterations. Increasing the training iterations from 186K to 372K further improves the performance by 0.2%. All reported results are obtained without ImageNet [51] pretraining.

Correlation Analysis. We sampled 10 subnetworks, training each from scratch for 40,000 iterations. The results, shown in Table 1, reveal a high correlation between the mIoU scores within the supernet and after retraining, with a Kendall’s τ of 0.58 and a Pearson Correlation Coefficient (ρ) of 0.79. This strong correlation confirms our ability to identify high-performing subnetworks within the supernet. Moreover, our search method not only reduces search and GPU memory costs compared to state-of-the-art methods but also efficiently yields multiple viable architectures from a single search process.

4.6. Visualization

We visualize our predictions in Figure 5. It is obvious to see that our predictions are accurate on fine-grained details thanks to our high resolution representation learning with attention.

5. Limitations

Although our HyCTAS framework achieves state-of-the-art speed and accuracy trade-offs in semantic and panoptic segmentation, several limitations



Figure 5: Visualization on COCO and Cityscapes validation set. The first row corresponds to COCO original images and the second row presents their semantic segmentation results. The third row corresponds to Cityscapes original images and the fourth row presents their semantic segmentation results. Best viewed in color.

remain:

- **Sensitivity to Noise and Occlusions.** Our method, like most deep architectures, can degrade in highly noisy or heavily occluded scenarios. Future work could integrate robust loss functions or data augmentation targeted at severe occlusions.
- **Extreme Resolution Shifts.** While our multi-resolution branches handle moderate scale variations, extremely large input images or drastic changes in scale may still pose memory challenges, even with our memory-efficient attention.
- **Domain Generalization.** We have mainly evaluated on well-known datasets such as Cityscapes and ADE20K. In real-world applications (e.g., certain industrial or medical imaging domains), domain shifts could undermine performance if the training distribution differs substantially.

We plan to investigate these aspects in future research, potentially by extending our search space to incorporate more robust modules or domain-adaptive strategies.

6. Conclusion

In this paper, we propose a novel HyCTAS framework to search for efficient networks with high-resolution representation and attention. We introduce a lightweight convolution module to reduce computation costs while preserving high-resolution information and a memory-efficient self-attention module to capture long-range dependencies. By combining a multi-branch search space and an efficient genetic search algorithm with multiple objectives, our searched architectures not only fuse features from selective branches for efficiency but also maintain high-resolution representations for performance. Additionally, the discovered architecture provides insights into how to use self-attention when designing new networks. Extensive experiments demonstrate that HyCTAS outperforms previous methods in both semantic segmentation and panoptic segmentation tasks while significantly improving inference speed. Future work will focus on applying this approach to more challenging tasks, such as key-point localization and object detection.

Acknowledgement

This work is jointly supported by National Key Research and Development Program of China (2016YFB1001000), National Natural Science Foundation of China (61525306, 61633021, 61721004, 61420106015, 61806194), Capital Science and Technology Leading Talent Training Project (Z181100006318030), and Beijing Science and Technology Project (Z181100008918010).

Author Contributions

H. Yu conceived the initial idea, designed the supernet, and conducted the majority of experiments. **C. Wan** and **X. Dai** contributed to the multi-objective

search algorithm implementation and code maintenance. **M. Liu, D. Chen**, and **B. Xiao** provided guidance on memory-efficient self-attention design and revised the manuscript. **Y. Huang, Y. Lu**, and **L. Wang** brought expertise in high-resolution networks, coordinated the experimental setup, and offered theoretical insights on multi-branch architectures. All authors reviewed the paper, discussed experiments, and approved the final manuscript.

References

References

- [1] K. He, G. Gkioxari, P. Dollár, R. Girshick, Mask r-cnn, in: ICCV, 2017.
- [2] D. Zhang, G. Huang, Q. Zhang, J. Han, J. Han, Y. Yu, Cross-modality deep feature learning for brain tumor segmentation, Pattern Recognition 110 (2021) 107562.
- [3] B. Cheng, B. Xiao, J. Wang, H. Shi, T. S. Huang, L. Zhang, Higherhrnet: Scale-aware representation learning for bottom-up human pose estimation, in: CVPR, 2020.
- [4] K. Sun, Y. Zhao, B. Jiang, T. Cheng, B. Xiao, D. Liu, Y. Mu, X. Wang, W. Liu, J. Wang, High-resolution representations for labeling pixels and regions, arXiv:1904.04514.
- [5] J. Wang, K. Sun, T. Cheng, B. Jiang, C. Deng, Y. Zhao, D. Liu, Y. Mu, M. Tan, X. Wang, et al., Deep high-resolution representation learning for visual recognition, IEEE transactions on pattern analysis and machine intelligence 43 (10) (2020) 3349–3364.
- [6] C. Liu, L.-C. Chen, F. Schroff, H. Adam, W. Hua, A. L. Yuille, L. Fei-Fei, Auto-deeplab: Hierarchical neural architecture search for semantic image segmentation, in: CVPR, 2019.
- [7] W. Chen, X. Gong, X. Liu, Q. Zhang, Y. Li, Z. Wang, Fasterseg: Searching for faster real-time semantic segmentation, in: ICLR, 2020.

- [8] H. Wu, J. Zhang, K. Huang, Sparsemask: Differentiable connectivity learning for dense image prediction, in: ICCV, 2019.
- [9] L.-C. Chen, M. D. Collins, Y. Zhu, G. Papandreou, B. Zoph, F. Schroff, H. Adam, J. Shlens, Searching for efficient multi-scale architectures for dense image prediction, in: NeurIPS, 2018.
- [10] V. Nekrasov, H. Chen, C. Shen, I. Reid, Fast neural architecture search of compact semantic segmentation models via auxiliary cells, in: CVPR, 2019.
- [11] A. Dosovitskiy, L. Beyer, A. Kolesnikov, D. Weissenborn, X. Zhai, T. Unterthiner, M. Dehghani, M. Minderer, G. Heigold, S. Gelly, J. Uszkoreit, N. Houlsby, An image is worth 16x16 words: Transformers for image recognition at scale, in: ICLR, 2021.
- [12] S. Zheng, J. Lu, H. Zhao, X. Zhu, Z. Luo, Y. Wang, Y. Fu, J. Feng, T. Xiang, P. H. Torr, L. Zhang, Rethinking semantic segmentation from a sequence-to-sequence perspective with transformers, in: CVPR, 2021.
- [13] J. Long, E. Shelhamer, T. Darrell, Fully convolutional networks for semantic segmentation, in: CVPR, 2015.
- [14] L.-C. Chen, G. Papandreou, I. Kokkinos, K. Murphy, A. L. Yuille, Deeplab: Semantic image segmentation with deep convolutional nets, atrous convolution, and fully connected crfs, IEEE transactions on pattern analysis and machine intelligence 40 (4) (2017) 834–848.
- [15] H. Zhao, X. Qi, X. Shen, J. Shi, J. Jia, Icnet for real-time semantic segmentation on high-resolution images, in: ECCV, 2018.
- [16] C. Yu, J. Wang, C. Peng, C. Gao, G. Yu, N. Sang, Bisenet: Bilateral segmentation network for real-time semantic segmentation, in: ECCV, 2018.
- [17] R. P. Poudel, S. Liwicki, R. Cipolla, Fast-scnn: fast semantic segmentation network, in: BMVC, 2019.

- [18] A. Howard, M. Sandler, G. Chu, L.-C. Chen, B. Chen, M. Tan, W. Wang, Y. Zhu, R. Pang, V. Vasudevan, et al., Searching for mobilenetv3, in: ICCV, 2019.
- [19] Q. Wan, Z. Huang, J. Lu, G. Yu, L. Zhang, Seaformer: Squeeze-enhanced axial transformer for mobile semantic segmentation, arXiv preprint arXiv:2301.13156.
- [20] M. Poyser, T. P. Breckon, Neural architecture search: A contemporary literature review for computer vision applications, Pattern Recognition 147 (2024) 110052.
- [21] M. Tan, B. Chen, R. Pang, V. Vasudevan, M. Sandler, A. Howard, Q. V. Le, Mnasnet: Platform-aware neural architecture search for mobile, in: CVPR, 2019.
- [22] H. Liu, K. Simonyan, Y. Yang, Darts: Differentiable architecture search, in: ICLR, 2019.
- [23] Y. Zhang, Z. Qiu, J. Liu, T. Yao, D. Liu, T. Mei, Customizable architecture search for semantic segmentation, in: CVPR, 2019.
- [24] Y. Li, L. Song, Y. Chen, Z. Li, X. Zhang, X. Wang, J. Sun, Learning dynamic routing for semantic segmentation, in: CVPR, 2020.
- [25] A. Vaswani, N. Shazeer, N. Parmar, J. Uszkoreit, L. Jones, A. N. Gomez, L. Kaiser, I. Polosukhin, Attention is all you need, in: NeurIPS, 2017.
- [26] N. Carion, F. Massa, G. Synnaeve, N. Usunier, A. Kirillov, S. Zagoruyko, End-to-end object detection with transformers, in: ECCV, 2020.
- [27] J. Yu, L. Yang, N. Xu, J. Yang, T. Huang, Slimmable neural networks, in: ICLR, 2019.
- [28] Y. Yuan, X. Chen, J. Wang, Object-contextual representations for semantic segmentation, in: ECCV, 2020.

- [29] L. Li, A. Talwalkar, Random search and reproducibility for neural architecture search, in: *UAI*, 2019.
- [30] K. Deb, A. Pratap, S. Agarwal, T. Meyarivan, A fast and elitist multi-objective genetic algorithm: Nsga-ii, *IEEE transactions on evolutionary computation* 6 (2) (2002) 182–197.
- [31] A. Kirillov, R. Girshick, K. He, P. Dollár, Panoptic feature pyramid networks, in: *CVPR*, 2019.
- [32] M. Cordts, M. Omran, S. Ramos, T. Rehfeld, M. Enzweiler, R. Benenson, U. Franke, S. Roth, B. Schiele, The cityscapes dataset for semantic urban scene understanding, in: *CVPR*, 2016.
- [33] T.-Y. Lin, M. Maire, S. Belongie, J. Hays, P. Perona, D. Ramanan, P. Dollár, C. L. Zitnick, Microsoft coco: Common objects in context, in: *ECCV*, 2014.
- [34] B. Zhou, H. Zhao, X. Puig, S. Fidler, A. Barriuso, A. Torralba, Scene parsing through ade20k dataset, in: *CVPR*, 2017.
- [35] B. Cheng, M. D. Collins, Y. Zhu, T. Liu, T. S. Huang, H. Adam, L.-C. Chen, Panoptic-deeplab: A simple, strong, and fast baseline for bottom-up panoptic segmentation, in: *CVPR*, 2020.
- [36] X. Li, Y. Zhou, Z. Pan, J. Feng, Partial order pruning: for best speed/accuracy trade-off in neural architecture search, in: *CVPR*, 2019.
- [37] A. Shaw, D. Hunter, F. Landola, S. Sidhu, Squeezenas: Fast neural architecture search for faster semantic segmentation, in: *ICCVW*, 2019.
- [38] J. Li, A. Raventos, A. Bhargava, T. Tagawa, A. Gaidon, Learning to fuse things and stuff, *arXiv preprint arXiv:1812.01192*.
- [39] Y. Li, X. Chen, Z. Zhu, L. Xie, G. Huang, D. Du, X. Wang, Attention-guided unified network for panoptic segmentation, in: *CVPR*, 2019.

- [40] Y. Xiong, R. Liao, H. Zhao, R. Hu, M. Bai, E. Yumer, R. Urtasun, Upsnet: A unified panoptic segmentation network, in: CVPR, 2019.
- [41] L. Porzi, S. R. Bulo, A. Colovic, P. Kortschieder, Seamless scene segmentation, in: CVPR, 2019.
- [42] K. Sofiuk, O. Barinova, A. Konushin, Adaptis: Adaptive instance selection network, in: ICCV, 2019.
- [43] T.-J. Yang, M. D. Collins, Y. Zhu, J.-J. Hwang, T. Liu, X. Zhang, V. Sze, G. Papandreou, L.-C. Chen, Deeperlab: Single-shot image parser, arXiv preprint arXiv:1902.05093.
- [44] N. Gao, Y. Shan, Y. Wang, X. Zhao, Y. Yu, M. Yang, K. Huang, Ssap: Single-shot instance segmentation with affinity pyramid, in: ICCV, 2019.
- [45] H. Zhao, J. Shi, X. Qi, X. Wang, J. Jia, Pyramid scene parsing network, in: CVPR, 2017.
- [46] L.-C. Chen, Y. Zhu, G. Papandreou, F. Schroff, H. Adam, Encoder-decoder with atrous separable convolution for semantic image segmentation, in: ECCV, 2018.
- [47] E. Xie, W. Wang, Z. Yu, A. Anandkumar, J. M. Alvarez, P. Luo, Segformer: Simple and efficient design for semantic segmentation with transformers, in: NeurIPS, 2021.
- [48] H. Zhang, K. Dana, J. Shi, Z. Zhang, X. Wang, A. Tyagi, A. Agrawal, Context encoding for semantic segmentation, in: CVPR, 2018.
- [49] K. He, X. Zhang, S. Ren, J. Sun, Deep residual learning for image recognition, in: CVPR, 2016.
- [50] M. Sandler, A. Howard, M. Zhu, A. Zhmoginov, L.-C. Chen, Mobilenetv2: Inverted residuals and linear bottlenecks, in: CVPR, 2018.
- [51] J. Deng, W. Dong, R. Socher, L.-J. Li, K. Li, L. Fei-Fei, Imagenet: A large-scale hierarchical image database, in: CVPR, 2009.